Electronic Properties of Molecules and Surfaces with a Self-Consistent Interatomic van der Waals Density Functional

Nicola Ferri[1], Robert A. DiStasio Jr.[2], Alberto Ambrosetti[1], Roberto Car[2], and Alexandre Tkatchenko[1]
[1] *Fritz-Haber-Institut der Max-Planck-Gesellschaft, Faradayweg 4-6, 14195, Berlin, Germany*
[2] *Department of Chemistry, Princeton University, Princeton, New Jersey 08544, USA*

How strong is the effect of van der Waals (vdW) interactions on the electronic properties of molecules and extended systems? To answer this question, we derived a fully self-consistent implementation of the density-dependent interatomic vdW functional of Tkatchenko and Scheffler [Phys. Rev. Lett. **102**, 073005 (2009)]. Not surprisingly, vdW self-consistency leads to tiny modifications of the structure, stability, and electronic properties of molecular dimers and crystals. However, unexpectedly large effects were found in the binding energies, distances and electrostatic moments of highly polarizable alkali metal dimers. Most importantly, vdW interactions induced complex and sizable electronic charge redistribution in the vicinity of metallic surfaces and at organic/metal interfaces. As a result, a substantial influence on the computed workfunctions was found, revealing a non-trivial connection between electrostatics and long-range electron correlation effects.

Ubiquitous in nature, van der Waals (vdW) interactions are the result of quantum mechanical fluctuations of the electron density, $n(\mathbf{r})$, and play a critical role in the formation, stability, and function of a wide variety of systems, ranging from simple noble-gas dimers to complex hybrid organic/inorganic interfaces [1–3]. Since the long-range vdW energy, $E_{\rm vdW}$, typically represents only a tiny fraction ($\sim 0.001\%$) of the total energy, the influence of vdW on $n(\mathbf{r})$ and electronic properties, such as multipolar moments and orbital energy levels, is commonly assumed to be rather small, if not negligible. For this reason, some of the most widely used methodologies for incorporating vdW interactions within the framework of density-functional theory (DFT), are generally approximated by an *a posteriori* perturbation of the total energy, and are therefore only accounted for after $n(\mathbf{r})$ has been obtained via the self-consistent (SC) solution of the nonlinear Kohn-Sham (KS) equations.

In a fully SC scheme, the contribution of the electronic vdW potential, $v_{\rm vdW}[n(\mathbf{r})] = \delta E_{\rm vdW}[n(\mathbf{r})]/\delta n(\mathbf{r})$, *i.e.*, the functional derivative of the vdW energy with respect to the electron density, would be directly added to the exchange-correlation (XC) potential to form the total effective potential in the KS equations. In this regard, SC implementations are currently available for the nonlocal vdW-DF family of XC functionals resulting from the Chalmers/Rutgers collaboration [4–7], as well as the density-dependent dispersion correction (dDsC) of Steinmann and Corminboeuf [8, 9]. When applied to small atomic and molecular dimers, only slight modifications of the structure and stability, along with minuscule changes in $n(\mathbf{r})$, were found due to a SC treatment of both of these vdW-inclusive methods [6, 7, 10, 11]. However, while SC vdW effects are expected to produce modest structural and density changes in small molecular dimers, a rigorous investigation of these electron density modifications, as well as a thorough analysis of larger and more complex systems, such as metallic surfaces and organic/inorganic interfaces, has still not been performed to date.

In this Letter, we report a fully SC implementation of the density-dependent interatomic vdW functional of Tkatchenko and Scheffler (vdW$^{\rm TS}$) [12]. The effects of a SC treatment of long-range vdW interactions on $n(\mathbf{r})$ are subsequently assessed in small molecular dimers, alkali metal dimers, transition-metal surfaces, and organic/metal interfaces, finding unexpectedly large effects in the electronic properties for many of these systems.

Based on a pairwise-additive summation of interatomic dispersion contributions, an efficient and widely used approach for incorporating vdW interactions in DFT [12–15], the density-dependent vdW$^{\rm TS}$ energy expression is given as [12]:

$$E_{\rm vdW^{TS}}[n(\mathbf{r})] = -\frac{1}{2}\sum_{AB} f_{AB}[n(\mathbf{r})]C_{6,AB}[n(\mathbf{r})]R_{AB}^{-6}\,, \quad (1)$$

in which $R_{AB} = |\mathbf{R}_A - \mathbf{R}_B|$ is the distance between atoms A and B, $C_{6,AB}[n(\mathbf{r})]$ is the corresponding dipole-dipole vdW coefficient, and $f_{AB}[n(\mathbf{r})] = f_{AB}(R_{AB}, R^0_{AB}[n(\mathbf{r})])$ is a Fermi-type damping function introduced to avoid the divergence of R_{AB}^{-6} for small interatomic distances and to couple the long-range vdW energy to a given semi-local XC functional *via* the correlation length defined by $R^0_{AB}[n(\mathbf{r})]$, the sum of the vdW radii associated with atoms A and B. In the vdW$^{\rm TS}$ scheme, the explicit dependence on $n(\mathbf{r})$ originates from the *effective* quantities in Eq. (1) above, $C_{6,AB}[n(\mathbf{r})] \equiv \gamma_A[n(\mathbf{r})]\gamma_B[n(\mathbf{r})]C^{\rm free}_{6,AB}$ and $R^0_{AB}[n(\mathbf{r})] \equiv (\gamma_A[n(\mathbf{r})])^{1/3} R_A^{0,\rm free} + (\gamma_B[n(\mathbf{r})])^{1/3} R_B^{0,\rm free}$, which are defined utilizing the following volume ratio,

$$\gamma_A[n(\mathbf{r})] = \frac{V_A[n(\mathbf{r})]}{V_A^{\rm free}} = \frac{\int d\mathbf{r}\, r^3 w_A(\mathbf{r}) n(\mathbf{r})}{\int d\mathbf{r}\, r^3 n_A^{\rm free}(\mathbf{r})}\,, \quad (2)$$

wherein $w_A(\mathbf{r}) = n_A^{\rm free}(\mathbf{r}) / \sum_B n_B^{\rm free}(\mathbf{r})$ is the Hirshfeld [16] weight for partitioning the total charge density into atomic components, in conjunction with free-atom reference data (taken from experiment and high-

level quantum chemical calculations) to account for hybridization, Pauli repulsion, and other semi-local XC effects in the construction of these quantities for a given "atom-in-a-molecule".

The vdW potential—the main ingredient in a SC implementation—has been derived analytically in this work and is comprised of the following terms,

$$v_{\mathrm{vdW^{TS}}}[n(\mathbf{r})] = -\frac{1}{2}\sum_{AB}\left[\left(\frac{\delta f_{AB}[n(\mathbf{r})]}{\delta n(\mathbf{r})}\right)C_{6,AB}[n(\mathbf{r})]R_{AB}^{-6} + f_{AB}[n(\mathbf{r})]\left(\frac{\delta C_{6,AB}[n(\mathbf{r})]}{\delta n(\mathbf{r})}\right)R_{AB}^{-6}\right], \quad (3)$$

and therefore includes the functional derivatives corresponding to both of the aforementioned quantities that explicitly depend on $n(\mathbf{r})$. As mentioned above, the electronic vdW potential given in Eq. (3) would be directly added to the XC potential to form the total KS effective potential, *i.e.*, $v[n(\mathbf{r})] = v_{\mathrm{XC}}[n(\mathbf{r})] + v_{\mathrm{vdW^{TS}}}[n(\mathbf{r})]$, which will modify the single-particle eigenfunctions and eigenvalues resulting from a SC solution of the electronic KS equations. In what follows, we will refer to this SC vdW scheme as DFA+vdW$_{\mathrm{sc}}^{\mathrm{TS}}$, in which DFA represents the underlying approximate XC functional utilized. The DFA+vdW$_{\mathrm{sc}}^{\mathrm{TS}}$ methodology has been implemented for both periodic and non-periodic systems in the full-potential all-electron code, FHI-aims [17], which has been employed for all of the calculations reported herein, and in the plane-wave and pseudopotential based code, Quantum ESPRESSO [18, 19].

We first apply this method to the methane (CH_4) dimer, separated along the z-axis by a fixed carbon-carbon distance of 6.72 Å. To evaluate the density response due to the inclusion of long-range correlation effects, we considered a series of electron density differences as a function of z (by integrating over the corresponding orthogonal x-y planes), *i.e.*, $\Delta n_{\mathrm{M1-M2}}(z) = \int\int dx\,dy\,[n_{\mathrm{M1}}(\mathbf{r}) - n_{\mathrm{M2}}(\mathbf{r})]$, in which M1 and M2 refer to the different electronic structure methods employed (See Fig. 1). As a reference, we have computed $\Delta n_{\mathrm{CCSD-HF}}(z)$, the integrated electron density difference between the coupled-cluster single and double excitations level of theory (CCSD) and the underlying mean-field Hartree-Fock (HF) approximation [20]. Here we note that the performance of the PBE [21] and HF methodologies coupled with vdW$_{\mathrm{sc}}^{\mathrm{TS}}$ match almost perfectly with the reference $\Delta n_{\mathrm{CCSD-HF}}(z)$, which is strongly indicative that the vdW$_{\mathrm{sc}}^{\mathrm{TS}}$ scheme correctly captures the response of the long-range vdW energy with respect to $n(\mathbf{r})$ (*i.e.*, the second term in Eq. (3)). In addition, both of these methods display identical shapes over the entire z-range, which is further evidence of the robustness of the vdW$_{\mathrm{sc}}^{\mathrm{TS}}$ correction with respect to the underlying XC functional. In the region between the methane molecules, the inclusion of vdW$_{\mathrm{sc}}^{\mathrm{TS}}$ produces a positive $\Delta n(z)$, with an accumulated density that decays with a slope similar to $\Delta n_{\mathrm{CCSD-HF}}(z)$.

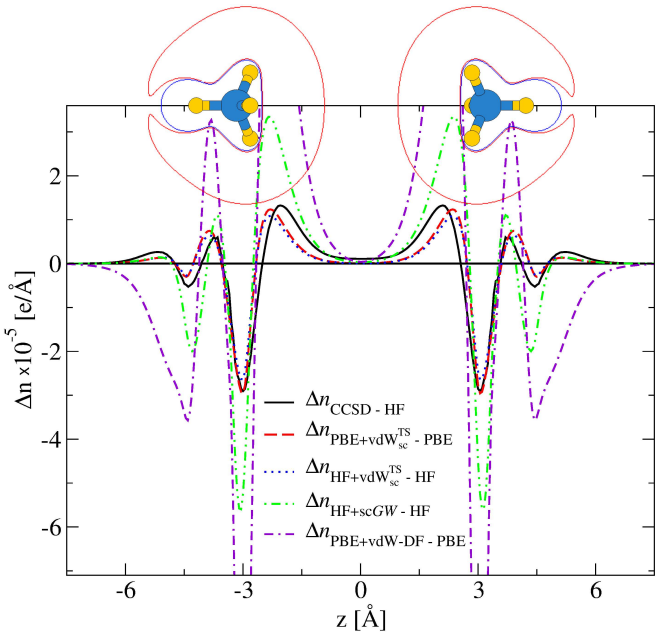

FIG. 1. Integrated electron density differences ($\Delta n(z)$) for the methane (CH_4) dimer separated by a carbon-carbon distance of 6.72 Å along the z-axis. The molecular geometry of the methane dimer is sketched along with the 2-D isodensity surfaces produced by the $\Delta n_{\mathrm{PBE+vdW_{sc}^{TS}-PBE}}(z)$ electron density difference. The outer/inner contours delimit regions of electron density accumulation/depletion ($\pm 10^{-7}$ e/Å^3). Truncated for clarity, the $\Delta n_{\mathrm{PBE+vdW-DF-PBE}}(z)$ electron density difference varies from -14×10^{-5} to 9×10^{-5} e/Å.

The challenges associated with reproducing the vdW-induced changes in $n(\mathbf{r})$ are highlighted by considering the self-consistent *GW* (sc-*GW*) methodology [22]. While the density difference $\Delta n_{\mathrm{HF+sc}GW-\mathrm{HF}}(z)$ captures all of the qualitative features of the reference $\Delta n_{\mathrm{CCSD-HF}}(z)$, there still remain quantitative differences in the magnitude and decay rate of the density modifications. While such differences might be attributed to the overestimation of C_6 coefficients at the sc-*GW* level of theory, these discrepancies are indicative of the high level of accuracy that is required in order to correctly capture the non-trivial density modifications induced by long-range correlation effects. Similar to the sc-*GW* method, the SC vdW-DF functional also reproduces the shape of the $n(\mathbf{r})$ redistribution, but yields much larger charge rearrangements than the CCSD reference. Since the vdW-DF C_6 coefficient for the methane dimer is accurate [23], this overestimation must stem from the large-gradient behavior of the vdW-DF kernel.

All of the curves in Fig. 1 show a redistribution of $n(\mathbf{r})$ in which two accumulation peaks develop in the region between the molecules due to the inclusion of long-range correlation effects. This net accumulation of charge density produces an electrostatic attraction between the nu-

clear framework of a given molecule and its own distorted electronic cloud, leading to an "effective" intermolecular attraction. Hence, this analysis of SC vdW effects provides a clear connection between the Feynman picture, in which vdW interactions stem from the electrostatic attraction between perturbed molecular electron densities [24] and the more conventional London approach, in which vdW interactions result from the electrodynamic coupling between fluctuating molecular dipoles.

Considering now the influence of a SC vdW treatment on the binding energies for a large variety of systems, ranging from small gas-phase dimers to systems of increasing complexity and size *e.g.*, the S22 database [25], the X23 database of molecular crystals [26], as well as metal surfaces, we found that the SC and *a posteriori* treatments provide nearly consistent binding energies in general, with differences spanning from a negligible 0.001% in the Ar dimer to just under 1% in extended metal surfaces. We note here that a SC treatment of vdW interactions can in fact lead to significantly larger changes (on the order of 5%) in the different components of the total electronic energy, such as the kinetic and Hartree contributions, but in most cases these energetic modifications largely cancel out, yielding a negligible difference in the final binding energy. However, substantially larger effects will intervene in polarizable systems with strong vdW effects, such as the alkali metal dimers. In this regard, we computed the binding energy curves for Cs$\cdots$Cs and Na$\cdots$Cs using the HF+vdW$^{\rm TS}_{\rm sc}$ and HF+vdW$^{\rm TS}$ methods. In both cases, the SC vdW method improves the agreement of structural, energetic, and electronic properties with experiment. For Cs$\cdots$Cs, the equilibrium internuclear distance was increased from 4.50 to 4.58 Å (compared to the experimental value of 4.65 Å [27]), accompanied by an increase of 25 meV ($\sim$ 9%) in the binding energy. For the heteronuclear Na$\cdots$Cs, the binding distance was *decreased* by 0.08 Å, coupled with a significant increase of 35 meV ($\sim$ 40%) in the binding energy and a reduction of 0.73 Debye in the dipole moment, resulting in a computed value of 5.44 Debye (compared to the experimental value of 4.75±0.2 Debye [28]). We note in passing that the inclusion of semi-local PBE correlation only worsens the agreement with experiment for the electronic properties of these alkali metal dimers.

To study the effects of a SC treatment of vdW interactions on extended systems, we now employ the recent extension of the vdW$^{\rm TS}$ method to model adsorbates on surfaces, the vdW$^{\rm surf}$ scheme [29], which builds on Lifshitz-Zaremba-Kohn (LZK) theory to include the many-body collective electronic response of the substrate *via* C_6 coefficient renormalization [30, 31]. In analogy to the analysis performed above for the methane dimer, we consider the integrated electron density difference, $\Delta n_{\rm PBE+vdW^{surf}_{sc}-PBE}(z)$, along the z-axis defining the direction normal to the (111) surfaces of the most common

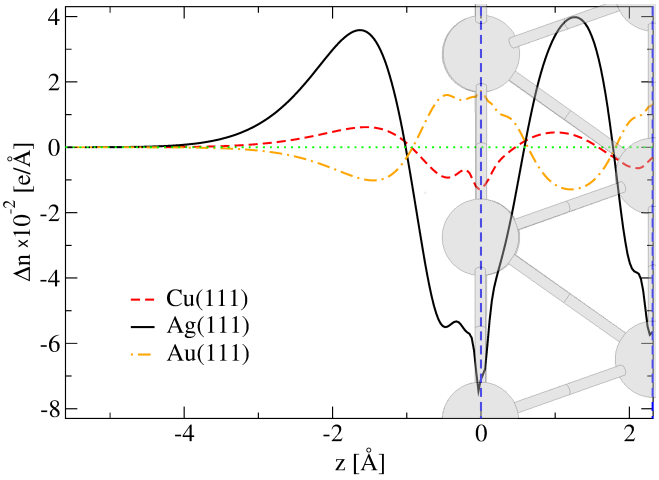

FIG. 2. Integrated electron density differences ($\Delta n(z)$) between the PBE+vdW$^{\rm surf}_{\rm sc}$ and PBE methods along the axis perpendicular to the (111) surfaces of a series of coinage metals. The vertical dashed line at $z = 0$ represents the topmost metal layer with the vacuum to the left.

coinage metals: Cu, Ag, and Au (See Fig. 2). In doing so, the first point to highlight here is the fact that the $n(\mathbf{r})$ modifications for extended metal surfaces are roughly three orders of magnitude larger than in the gas-phase molecular dimers, which is strongly indicative of the importance of a SC vdW treatment in these systems.

For the Cu and Ag surfaces, there is a net accumulation of $n(\mathbf{r})$ between the metal layers and in the vacuum region, coupled with a depletion at the metal layers. On the contrary, the SC vdW ansatz yields an accumulation of $n(\mathbf{r})$ at the metal layers and a net depletion in the interstitial and vacuum regions in Au. These qualitatively opposing effects are due to the relative balance between the interatomic distance, a_0, and the vdW radius, R^0, of the metal in question. When $R^0 < a_0$, as is the case for Cu and Ag, the contribution from the vdW potential is dominated by the second term in Eq. (3), which redistributes $n(\mathbf{r})$ by depleting regions with a large concentration of the charge density. In the opposite case, when $R^0 \geq a_0$, as for Au, the damping regime plays a more important role, in which the relative importance of the first term in Eq. (3) increases, and eventually results in a switch of the accumulation/depletion regions. At large distances from the metal surface, *i.e.*, well into the vacuum region, the effects of the vdW potential on $n(\mathbf{r})$ decay as $1/(R-R_p)^3$ relative to the reference plane, R_p, as predicted by LZK theory [31].

As shown in Fig. 2, the SC vdW effects on $n(\mathbf{r})$ primarily involve the topmost metal layer and the vacuum region, suggesting that the vdW potential is significantly modifying the surface dipole of these metals. In this regard, an observable property that is directly related to the surface dipole is the workfunction, Φ, defined as the minimum energy required to displace an electron from

TABLE I. Workfunctions (in eV) of various metal (111) surfaces obtained from experiment [36–38] and theory using the PBE and PBE+vdW$_{\rm sc}^{\rm surf}$ methodologies. The experimental methods utilized to obtain these workfunctions are denoted by PE (photoelectric effect) or FE (field emission). Underlined values denote cases with the largest vdW$_{\rm sc}^{\rm surf}$ effects.

Metal	Period	Experiment [Method]	PBE	PBE+vdW$_{\rm sc}^{\rm surf}$
Cu	4	4.94 [PE]	<u>4.89</u>	<u>4.95</u>
Rh	5	5.60 [PE]	<u>5.26</u>	<u>5.55</u>
Ag	5	4.74 [PE]	<u>4.44</u>	<u>4.74</u>
Ir	6	5.76 [PE]	5.66	5.64
Pt	6	5.93 [FE]	5.76	5.73
Au	6	5.32 [PE]	5.18	5.14

the metal surface to the vacuum, *i.e.*, $\Phi = V_{\rm vac} - E_F$, in which $V_{\rm vac}$ is the electrostatic potential in the vacuum region and E_F is the Fermi energy. Hence, the experimentally and theoretically determined workfunctions for six different metal (111) surfaces are listed in Table I. Each of these metal surfaces were constructed using lattice constants computed at the PBE+vdW$^{\rm surf}$ level of theory [32], and the scaled zeroth-order regular approximation (ZORA) [33] was included to account for scalar relativistic effects. The resulting PBE workfunctions were in good agreement with previously obtained results [34, 35].

For those metals belonging to the fourth and fifth periods, the vdW$_{\rm sc}^{\rm surf}$ method increases the magnitude of Φ with respect to PBE and therefore improves the overall agreement with experiment, with particularly large effects found for both Rh and Ag. Since $R^0 < a_0$ in Rh, the same qualitative behavior found above for Cu and Ag occurs in this case (as shown in Fig. 2), namely, a net accumulation of $n(\mathbf{r})$ in the interstitial and vacuum regions coupled with a depletion within the metal layers. Consequently, E_F is lowered due to the attractive Coulombic interaction between the metal layers and the interstitial region, coupled with the formation of an increased surface dipole due to spillage of $n(\mathbf{r})$ into the vacuum region, increasing $V_{\rm vac}$. The combination of these two effects increases the workfunctions for Cu, Rh, and Ag as shown in Table I. In particular, the vdW$_{\rm sc}^{\rm surf}$ scheme modifies E_F by $\sim 6\%$ and $V_{\rm vac}$ by $\sim 40\%$ for Ag, resulting in a significant increase of 0.32 eV in Φ. In contrast to Cu, Rh, and Ag, the Pd atom has a fully occupied valence electron shell ([Kr]4d^{10}), exhibiting strong self-interaction error when using semi-local functionals. Therefore, we leave further analysis of the Pd(111) case for future work.

For the remaining three metals belonging to the sixth period (Ir, Pt, Au), Φ computed at the PBE level are slightly reduced in magnitude when SC vdW effects are included (See Table I). For these elements, $R^0 \geq a_0$ and the changes in $n(\mathbf{r})$ follow the behavior discussed above for Au. Here we observed a slightly increased E_F due to the vdW$_{\rm sc}^{\rm surf}$ scheme coupled with a small reduction of the corresponding PBE workfunctions (by 0.02–0.04 eV), with similar effects noticed when using hybrid functionals for Ir, Pt, and Au. With average discrepancies of 0.2 eV still remaining from experiment, it is well known that effects beyond the scalar relativistic approximation become increasingly more important in computing Φ for such heavy metals. In this regard, spin-orbit coupling (SOC) stabilizes the Fermi level of bulk Au by approximately 0.4 eV [39] which will in turn increase Φ. Hence, quantitative prediction of Φ in these systems will require a fully self-consistent surface calculation which accounts for both vdW and full relativistic effects.

To assess the general validity of our conclusions for metal surfaces, we further investigated the workfunctions of the Cu, Ag, and Au surfaces using the SC vdW-DF approach coupled with the PBE functional. Again we arrived at similar conclusions as found with PBE+vdW$_{\rm sc}^{\rm surf}$, namely an increase of Φ with the inclusion of SC vdW interactions, with the vdW-DF method yielding Φ values of 5.10, 4.78 and 5.40 eV for the Cu, Ag, and Au surfaces, respectively. These slight overestimates with respect to experiment are consistent with our findings above for the vdW-DF treatment of the methane dimer in Fig. 1.

The workfunctions of surfaces can be tuned by molecular adsorption, with vdW interactions playing a prominent role in the structure and stability of hybrid inorganic/organic systems (HIOS) [29, 40]. Since the Φ of HIOS are known to be very sensitive to adsorption, we extend our analysis of SC vdW effects by considering the following HIOS: the adsorption of benzene, diindenoperylene (DIP), and PTCDA on the Ag(111) surface. When compared to the corresponding clean surface, we found that the combined molecule/surface Φ decreased by 0.14, 0.21, and 0.22 eV, respectively, upon inclusion of SC vdW effects in these systems. In this regard, self-consistency systematically improves the agreement with the experimentally determined workfunctions in HIOS. However, the underlying mechanisms responsible for these observations are qualitatively different. For instance, the variation of Φ stems purely from the modification of the interface dipole for the benzene/Ag(111) HIOS, while the decrease in Φ is mainly due to an interplay between the interface dipole and a reduction in the charge transfer between the molecule and the surface for the HIOS involving larger aromatic molecules (*e.g.*, DIP and PTCDA).

In conclusion, we have developed and applied a fully self-consistent implementation of the Tkatchenko-Scheffler interatomic vdW functional within the framework of DFT. The developed SC scheme can also be extended to more advanced XC functionals based on the vdW$^{\rm TS}$ method, such as the iterative Hirshfeld [41] and many-body dispersion (MBD) [42] approaches, and will be addressed in future work. The analysis of SC vdW effects provided herein demonstrates a clear connection between the Feynman picture of vdW interactions originating from electrostatic attractions between perturbed

molecular electron densities and the more conventional London picture of vdW interactions. As an outcome of our comprehensive study, it is evident that the self-consistency of the vdW energy is particularly important in systems with high polarizability density and/or low dimensionality. The SC vdW effects can affect binding energies and molecular multipoles for polarizable fragments, surface dipoles and workfunctions for inorganic substrates, and interface dipoles and charge transfer for hybrid inorganic/organic systems. As such, our findings are also strongly suggestive of the potential importance of long-range vdW effects in properties beyond the electronic ground state.

We are grateful for support from the FP7 Marie Curie Actions of the European Commission, *via* the Initial Training Network SMALL (MCITN-238804), and the European Research Council (ERC) Starting Grant VDW-CMAT. R.D. and R.C. acknowledge support from the Scientific Discovery through Advanced Computing (SciDAC) program through the Department of Energy (DOE) under Grant No. DE-SC0008626. The authors would also like to acknowledge Prof. Matthias Scheffler, Prof. Volker Blum, Dr. Oliver Hofmann, and Dr. Viktor Atalla for helpful discussions.

[1] V. A. Parsegian, *Van der Waals Forces: A Handbook for Biologists, Chemists, Engineers and Physicists* (Cambridge University Press, 2005).
[2] A. J. Stone, *The Theory of Intermolecular Forces* (Oxford University Press, 1996).
[3] N. Nerngchamnong, L. Yuan, D.-C. Qi, J. Li, D. Thompson, and C. A. Nijhuis, Nat. Nanotechnol. **8**, 113 (2013).
[4] M. Dion, H. Rydberg, E. Schröder, D. C. Langreth, and B. I. Lundqvist, Phys. Rev. Lett. **92**, 246401 (2004).
[5] D. C. Langreth, M. Dion, H. Rydberg, E. Schröder, P. Hyldgaard, and B. I. Lundqvist, Int. J. Quantum Chem. **101**, 599 (2005).
[6] T. Thonhauser, V. R. Cooper, S. Li, A. Puzder, P. Hyldgaard, and D. C. Langreth, Phys. Rev. B **76**, 125112 (2007).
[7] D. C. Langreth, B. I. Lundqvist, S. D. Chakarova-Käc, V. R. Cooper, M. Dion, P. Hyldgaard, A. Kelkkanen, J. Kleis, L. Kong, S. Li, P. G. Moses, E. Murray, A. Puzder, H. Rydberg, E. Schröder, and T. Thonhauser, J. Phys. Cond. Matt. **21**, 084203 (2009).
[8] S. N. Steinmann and C. Corminboeuf, J. Chem. Phys. **134**, 044117 (2011).
[9] S. N. Steinmann and C. Corminboeuf, J. Chem. Theory Comput. **7**, 3567 (2011).
[10] M. Mura, A. Gulans, T. Thonhauser, and L. Kantorovich, Phys. Chem. Chem. Phys. **12**, 4759 (2010).
[11] É. Brémond, N. Golubev, S. N. Steinmann, and C. Corminboeuf, J. Chem. Phys. **140**, 18A516 (2014).
[12] A. Tkatchenko and M. Scheffler, Phys. Rev. Lett. **102**, 073005 (2009).
[13] S. Grimme, J. Comput. Chem. **25**, 1463 (2004).
[14] S. Grimme, J. Comput. Chem. **27**, 1787 (2006).
[15] S. Grimme, J. Antony, S. Ehrlich, and H. Krieg, J. Chem. Phys. **132**, 154104 (2010).
[16] F. L. Hirshfeld, Theor. Chim. Acta **44**, 129 (1977).
[17] V. Blum, R. Gehrke, F. Hanke, P. Havu, V. Havu, X. Ren, K. Reuter, and M. Scheffler, Comput. Phys. Commun. **180**, 2175 (2009).
[18] P. Giannozzi, S. Baroni, N. Bonini, M. Calandra, R. Car, C. Cavazzoni, D. Ceresoli, G. L. Chiarotti, M. Cococcioni, I. Dabo, A. Dal Corso, S. de Gironcoli, S. Fabris, G. Fratesi, R. Gebauer, U. Gerstmann, C. Gougoussis, A. Kokalj, M. Lazzeri, L. Martin-Samos, N. Marzari, F. Mauri, R. Mazzarello, S. Paolini, A. Pasquarello, L. Paulatto, C. Sbraccia, S. Scandolo, G. Sclauzero, A. P. Seitsonen, A. Smogunov, P. Umari, and R. M. Wentzcovitch, J. Phys.: Condens. Matter **21**, 395502 (2009).
[19] R. A. DiStasio Jr., B. Santra, Z. Li, X. Wu, and R. Car, J. Chem. Phys. **141**, 084502 (2014).
[20] M. J. Frisch *et al.*, Gaussian Inc. Wallingford CT 2009.
[21] J. P. Perdew, K. Burke, and M. Ernzerhof, Phys. Rev. Lett. **77**, 3865 (1996).
[22] F. Caruso, P. Rinke, X. Ren, A. Rubio, and M. Scheffler, Phys. Rev. B **88**, 075105 (2013).
[23] O. A. Vydrov and T. Van Voorhis, Phys. Rev. A **81**, 062708 (2010).
[24] R. P. Feynman, Phys. Rev. **56**, 340 (1939).
[25] P. Jurečka, J. Šponer, J. Černý, and P. Hobza, Phys. Chem. Chem. Phys. **8**, 1985 (2006).
[26] A. M. Reilly and A. Tkatchenko, J. Chem. Phys. **139**, 024705 (2013).
[27] M. Raab, G. Höning, W. Demtröder, and C. R. Vidal, J. Chem. Phys. **76**, 4370 (1982).
[28] P. J. Dagdigian and L. Wharton, J. Chem. Phys. **57**, 1487 (1972).
[29] V. G. Ruiz, W. Liu, E. Zojer, M. Scheffler, and A. Tkatchenko, Phys. Rev. Lett. **108**, 146103 (2012).
[30] E. M. Lifshitz, Sov. Phys. JETP **2**, 73 (1956).
[31] E. Zaremba and W. Kohn, Phys. Rev. B **13**, 2270 (1976).
[32] W. Liu, V. G. Ruiz, G.-X. Zhang, B. Santra, X. Ren, M. Scheffler, and A. Tkatchenko, New J. Phys. **15**, 053046 (2013).
[33] E. van Lenthe, E. J. Baerends, and J. G. Snijders, J. Chem. Phys. **101**, 9783 (1994).
[34] N. E. Singh-Miller and N. Marzari, Phys. Rev. B **80**, 235407 (2009).
[35] J. L. F. Da Silva, C. Stampfl, and M. Scheffler, Surf. Sci **600**, 703 (2006).
[36] *Handbook of Chemistry and Physics 94th Edition* (David R. Lide, 2013-2014) available online at `http://www.hbcpnetbase.com`.
[37] G. R. Castro, H. Busse, U. Schneider, T. Janssens, and K. Wandelt, Phys. Scr. **T41**, 208 (1992).
[38] J. W. Niemantsverdriet, *Spectroscopy in Catalysis, An Introduction* (VCH, Weinheim, 1993).
[39] P. Romaniello and P. L. de Boeij, J. Chem. Phys. **122**, 164303 (2005).
[40] C. Bürker, N. Ferri, A. Tkatchenko, A. Gerlach, J. Niederhausen, T. Hosokai, S. Duhm, J. Zegenhagen, N. Koch, and F. Schreiber, Phys. Rev. B **87**, 165443 (2013).
[41] T. Bučko, S. Lebègue, J. G. Ángyán, and J. Hafner, J. Chem. Phys. **141**, 034114 (2014).
[42] A. Tkatchenko, R. A. DiStasio Jr., R. Car, and M. Scheffler, Phys. Rev. Lett. **108**, 236402 (2012).